

ON-LINE APPENDIX

Ostium Ratio Calculation

As shown in Fig 1A in the main text, calculating the OsR requires calculating the surfaces of the aneurysm ostium and the circumferential surface area of the parent artery. Three steps are required to obtain the surface data: 1) parent vessel reconstruction, which involves reconstructing the native (healthy, nondiseased) parent vessel from the intracranial aneurysm geometry; 2) ostium surface generation, which involves subtracting the aneurysm geometry from the native parent vessel to obtain the ostium surface; and 3) corresponding parent vessel isolation, which involves obtaining the corresponding parent artery section and subtracting the ostium surface area from it to isolate the corresponding parent vessel surface for OsR calculations (On-line Fig 1).

In step 1, the original aneurysm model surface geometry is used for input and Voronoi diagrams and centerlines of the aneurysm surface are calculated. The aneurysm model is then clipped at the aneurysm-parent artery attachment region using the associated centerlines. The Voronoi points are interpolated throughout the clipped region to fill the attachment region, which is used to reconstruct the parent vessel lumen, resulting in the native parent artery.¹

In step 2, the original aneurysm geometry is subtracted from the reconstructed native parent artery, resulting in the ostium surface; the area of this surface is calculated as A_{ostium} . In step 3, the corresponding parent artery section is first defined by drawing planes at the proximal and distal ends of the ostium surface on the native artery. The ostium surface is then subtracted from this parent artery section to obtain the corresponding parent artery surface for the OsR calculation; the area of this surface is calculated as A_{vessel} . Step 1 is performed using the open-source software package, Vascular Modeling Toolkit. Steps 2 and 3 are performed using STAR-CCM+ (Version 11.02; Siemens PLM Software, Plano, Texas). The 3-step procedure was followed for all 63 aneurysm geometries to obtain aneurysm ostium and corresponding parent artery surfaces, and the OsR was calculated from the obtained surfaces for each case.

FD Virtual Deployment Technique and Metal Coverage Rate and Pore Density Calculation

An in-house virtual stenting workflow (VSW) was used to deploy flow diverters in the aneurysm geometries.^{2,3} In previous studies, VSW-based FD deployments were found to be efficient and patient-optimized over existing virtual deployment techniques⁴⁻⁶ because of vessel-specific initiation and rapid FD deployment. As opposed to generic virtual deployment techniques with vessel-specific initiation, the VSW optimizes the FD deployment specific to the patient-specific aneurysm geometry and size of the FD. Rapid deployment enables the VSW to deploy FDs in aneurysm models within seconds as opposed to hours or even days for other methods.^{6,7} The VSW consists of 3 steps: 1) preprocessing, in which the parent vessel is isolated from the aneurysm geometry and a simplex mesh structure is generated with a maximum inscribed sphere diameter along the vessel centerline using vessel-specific initialization; 2) simplex mesh expansion, in which the simplex mesh undergoes radial expansion using mathematic forces and stops the deployment process when the deployed sim-

plex mesh has good apposition with the parent vessel wall; and 3) postprocessing, to map the FD pattern on the deployed simplex mesh and sweep the wires into the 3D structures. Algorithms for the VSW were developed in Matlab (8.1, R2013; MathWorks, Natick, Massachusetts). The aneurysm geometries and the known FD device size were used as input to the VSW, and FDs were virtually deployed in all 63 aneurysm cases in our study.

Metal coverage rate and pore density were calculated on the virtual FD-deployment results. The design of an FD is inherently different from that of traditional neurovascular stents, considering that the FD has a higher MCR (or low porosity) and lower pore density to enable effective flow diversion in the aneurysms.⁸ For patient-specific aneurysms, MCR and pore density are calculated across the aneurysmal neck with the deployed FD to capture its deployment and flow-diversion capabilities at the neck surface.⁹ MCR quantifies the relative area covered by the FD struts at the neck as opposed to the open space between the struts (pores), and pore density quantifies the number of pores per unit area.¹⁰ To calculate the MCR and pore density, we captured an image of FD-deployment results at the aneurysmal neck plane for each patient. Digital image processing was then performed to identify the relative area of FD struts and open space (pores), which quantified the MCR. To quantify pore density, the number of pores in the image was divided by the area of the image to obtain the number of pores per unit area. The images of FD deployment at the aneurysmal neck were obtained in STAR-CCM+, and a stand-alone algorithm was written to calculate the MCR and pore density on the basis of the image using Matlab.

Experimental Validation Metal Coverage Rate and Pore Density Calculations

To validate the MCR and pore density values obtained from simulating FD deployments using the VSW, we compared those values against experimental calculations based on physical FD deployments on silicone phantom models of 3 representative patient-specific internal carotid artery aneurysms (On-line Fig 2A). Three aneurysm cases were chosen representing a small, medium, and giant sidewall aneurysm, with aneurysm sizes of 5, 9, and 18 mm, respectively. We used a previously described lost-wax technique¹¹ to fabricate optically clear silicone phantom models for each case. The silicone models were re-imaged using an Infinix C-arm machine (Toshiba, Tokyo, Japan) to obtain accurate surface geometry of the aneurysms. The re-imaged aneurysms were segmented, again using the Vascular Modeling Toolkit, to obtain 3D surface geometries of the silicone phantoms. Using these re-imaged 3D aneurysm geometries, we measured the parent artery diameters as 2.5, 3.1, and 2.8 mm in the small, medium, and giant aneurysms, respectively. Accordingly, FDs of sizes 2.75×20 mm, 3.75×20 mm, and 3×25 mm were deployed in the small, medium, and giant ICA silicone models, respectively, by an experienced neurointerventionist to ensure uniform FD deployment in each model. The VSW algorithm was then used on the re-imaged 3D geometries of each aneurysm model to simulate the physical deployment of the FDs of the given sizes in the silicone and 3D models.

To obtain experimental values of the MCR and pore density for each case, we first obtained an image of the FD deployment at

the neck of the aneurysm. The FD wires were then traced to obtain the wire configuration in the image. The final MCR and pore density were calculated on this processed image. The workflow used for calculating the MCR and pore density is illustrated on a sample plane on the medium ICA phantom in On-line Fig 2B.

Values of MCR and pore density for experimental and VSW deployments are plotted in On-line Fig 3. The values of MCR and pore density obtained from virtual VSW deployment were close to the experimental values. The percentage error in MCR values of VSW with respect to the experimental values were 0.7%, 8.2%, and 7.6% for the small, medium, and giant ICA aneurysms, respectively. For pore density, the VSW showed a percentage error of 7.8%, 6.6%, and 6.8% with respect to experimental pore density values for small, medium, and giant ICA aneurysms, respectively.

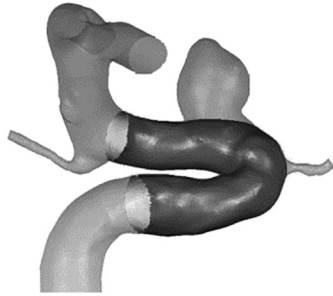
Measurements for Neck Ratio Calculations (D_1 and D_2)

Average measurements of D_1 in the occluded and residual groups were 3.84 ± 0.09 mm and 3.89 ± 0.17 mm, respectively. The average D_2 was 3.36 ± 0.08 mm in the occluded group and 3.66 ± 0.13 mm in the residual group. Even though there was tapering of the parent artery between the proximal and distal ends of the aneurysms in the measured D_1 and D_2 , these values were not statistically different in the occluded and residual groups (D_1 , $P = .77$; D_2 , $P = .08$).

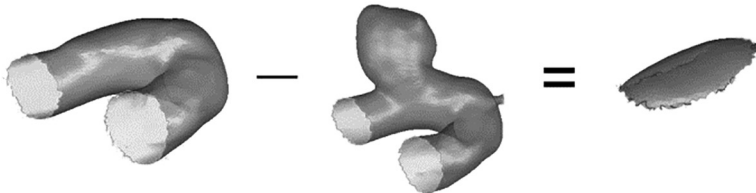
REFERENCES

1. Ford M, Hoi Y, Piccinelli M, et al. **An objective approach to digital removal of saccular aneurysms: technique and applications.** *Br J Radiol* 2009;82:S55–61 CrossRef Medline
2. Paliwal N, Yu H, Damiano R, et al. **Fast virtual stenting with vessel-specific initialization and collision detection.** In: *Proceedings of the ASME International Design Engineering Technical Conferences and Computers and Information in Engineering Conference*, Buffalo, New York. August 17–20, 2014; V003T12A14–V03T12A14
3. Paliwal N, Yu H, Xu J, et al. **Virtual stenting workflow with vessel-specific initialization and adaptive expansion for neurovascular stents and flow diverters.** *Comput Methods Biomech Biomed Eng* 2016;19:1423–31 CrossRef Medline
4. Appanaboyina S, Mut F, Löhner R, et al. **Simulation of intracranial aneurysm stenting: techniques and challenges.** *Comput Methods Appl Mech Eng* 2009;198:3567–82 CrossRef
5. Larrabide I, Kim M, Augsburger L, et al. **Fast virtual deployment of self-expandable stents: method and in vitro evaluation for intracranial aneurysmal stenting.** *Med Image Anal* 2012;16:721–30 CrossRef Medline
6. Ma D, Dargush GF, Natarajan SK, et al. **Computer modeling of deployment and mechanical expansion of neurovascular flow diverter in patient-specific intracranial aneurysms.** *J Biomech* 2012; 45:2256–63 CrossRef Medline
7. Bernardini A, Larrabide I, Morales HG, et al. **Influence of different computational approaches for stent deployment on cerebral aneurysm haemodynamics.** *Interface Focus* 2011;1:338–48 CrossRef Medline
8. Szikora I, Berentei Z, Kulcsar Z, et al. **Treatment of intracranial aneurysms by functional reconstruction of the parent artery: the Budapest experience with the Pipeline embolization device.** *AJNR Am J Neuroradiol* 2010;31:1139–47 CrossRef Medline
9. Lieber BB, Stancampiano AP, Wakhloo AK. **Alteration of hemodynamics in aneurysm models by stenting: influence of stent porosity.** *Ann Biomed Eng* 1997;25:460–69 CrossRef Medline
10. Lieber BB, Sadasivan C. **Endoluminal scaffolds for vascular reconstruction and exclusion of aneurysms from the cerebral circulation.** *Stroke* 2010;41:S21–25 CrossRef Medline
11. Paliwal N, Damiano RJ, Varble NA, et al. **Methodology for computational fluid dynamic validation for medical use: application to intracranial aneurysm.** *J Biomech Eng* 2017;139 CrossRef Medline

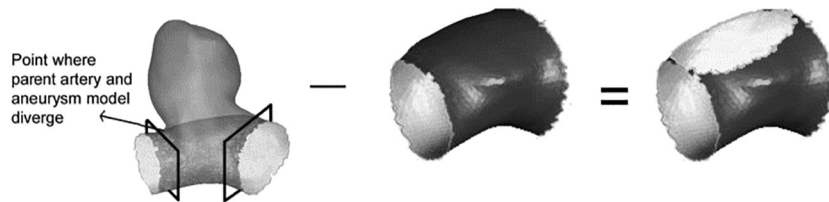
Step 1: Parent Vessel Reconstruction



Step 2: Ostium Surface Generation

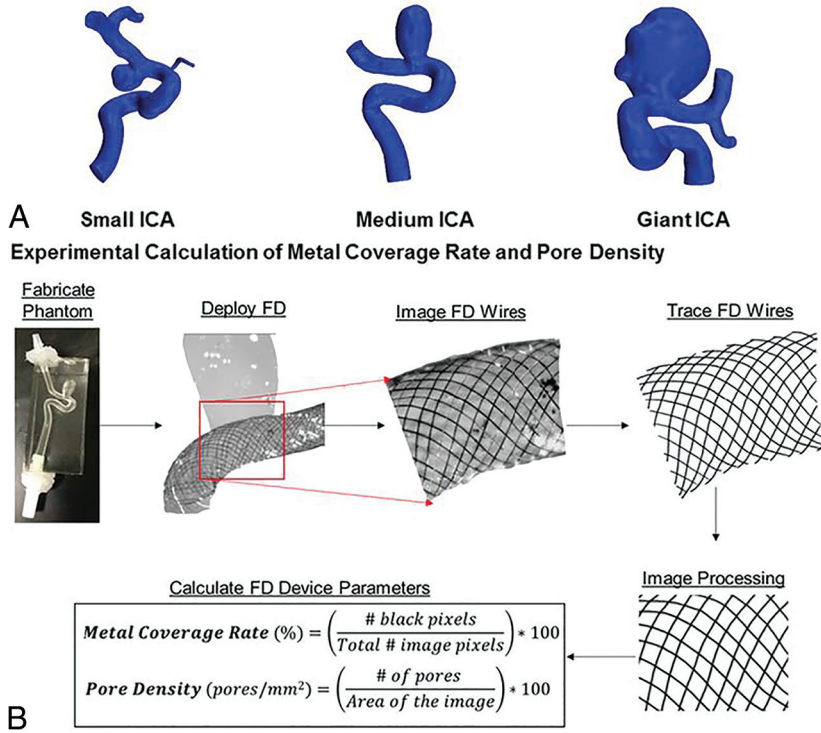


Step 3: Corresponding Parent Vessel Isolation

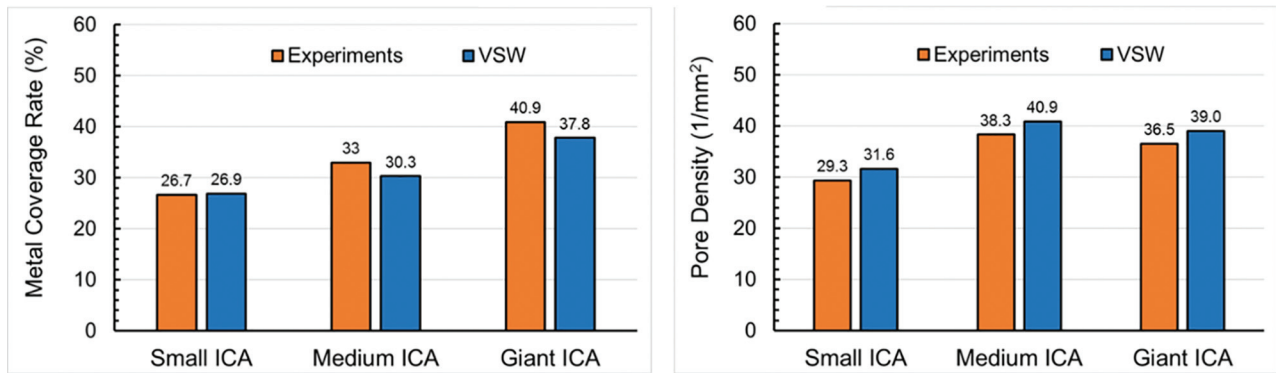


ON-LINE FIG 1. Workflow illustrating the 3-step procedure for obtaining aneurysm ostium and corresponding parent vessel surfaces from a representative aneurysm geometry.

Patient-Specific Aneurysm Models



ON-LINE FIG 2. Patient-specific aneurysm models and workflow used for quantifying MCR and pore density for validation analysis. A, Representative patient-specific aneurysm models for experimental validation of the VSW: small ICA (5 mm), medium ICA (9 mm), and giant ICA (18 mm) aneurysms. B, Illustration of the experimental workflow to calculate the MCR and pore density for experimental deployments on silicone phantoms for validation of the VSW.



ON-LINE FIG 3. Comparison of the MCR and pore density in the 3 representative aneurysm models between experimental (orange) and VSW (blue) deployments. The numbers on top of the graphs represent MCR and pore density values for each case.